Blucher Mechanical Engineering Proceedings
May 2014, vol. 1 , num. 1
www.proceedings.blucher.com.br/evento/10wccm

10th World Congress on Computational Mechanics
8-13 July 2012 • São Paulo • Brazil

AN OBJECT-ORIENTED UNSTEADY VORTEX LATTICE METHOD FOR AEROELASTIC ANALYSES OF HIGHLY FLEXIBLE WINGS.

C. E. de Souza[1], R. G. A. da Silva [2], C. E. S. Cesnik[3]

[1],[2] Institute of Aeronautics and Space, São José dos Campos (carlosesouza@gmail.com)

[3] Department of Aerospace Engineering, University of Michigan

Abstract.

This paper presents studies about aerodynamic modeling for aeroelastic analyses of composite laminated flexible wings subjected to large displacements. An unsteady vortex-lattice method (UVLM) is used, aiming reduction in computational costs when comparing with higher order CFD solutions. The UVLM has the advantage of being computationally simple, especially for complex configurations and for incompressible flow. Lifting surfaces subject to large angle of attack are very common in rotary wings area, but can also be important in the case of flapping wings in forward flight, where local fluid velocity components can lead to an effective angle of attack larger than the profile static stall limit. Since the vortex-lattice method is a potential method, without viscous effects, the boundary layer separation can not be captured. An engineering approach is then used to modify directly the pressure distribution based on an effective angle of attack calculated at each vortex-ring element. Applications to flat plate surfaces show good agreement with theory, and can predict hysteretic behavior in time response analyses. Application examples showing the ability to deal with multiple surfaces in rotary motion are also presented.

.

Keywords: *Unsteady Vortex-Lattice, stall model, large displacements, large rotations.*

1. INTRODUCTION

An unsteady vortex-lattice method (UVLM) formulation that adresses large displacements and rotations is presented. The formulation is implemented as a computational code, which is part of a wider nonlinear aeroelastic framework, presented in [7]. The problem of nonlinear aeroelasticity of highly flexible wings request a formulation capable of capture large structural displacements.

Different aerodynamic formulations were used in the large displacements problem investigation, including Peter's finite state methods [17] or Navier-Stokes [1] or Euler [13] formulations. The use of unsteady vortex-lattice methods (UVLM) has also been attempted, because of its implementation simplicity and moderate reduction in computational costs. Applications of UVLM to very flexible aircraft (VFA) wings are most often. In these cases, the

structural model is commonly represented by beam models, like a elastic beam coupled with rigid-body rotations [19] or geometrically-nonlinear composite beam [12]. [3] investigated the aeroelasticity of MAV with the use of a 3-D, free wake UVLM coupled with a membrane model with displacements calculated using Fourier series. Wings are simulated as membranes supported by a rigid frame in forward flight at a constant angle-of-attack (AoA). Stanford and Beran [15] couple the UVLM with a corotational FE to the investigation of flapping wings frame. The framework showed good results for structural response and aerodynamic forces prediction, even if not good for efficiency prediction. Later, this elements is used for design purposes [16], where accurate gradients comprise the most important aspect for optimization analysis. It is noted that the UVLM is unable to handle cases where the wing travel through previously generated wake, what means that the translation component in the wing plane must be large to allow the process of wake shedding at the trailing edge.

In forward flight of flexible wings, local angle of attack can achieve values above the profile static stall limit even for moderate displacements. This situation brings difficulties to the aeroelastic problem using UVLM due to the nature of stall. The stall is related with viscous flow separation over a lifting surface at high angles of attack. On the other hand, a potential based solution such as the UVLM is not an adequate model for representing separation effects.

As an approach applied to standard VLM, Ref. [9] uses experimental data to take into account viscous effects that dominate the separated flow. A separated vortex ring element was implemented, covering an area that begins at the separation point and goes until the reattachment point. This methodology, however, requires preliminary studies about the wing profile being analyzed, since chordwise separation lines must be known. Also, in [9] the simulations were all performed for steady stalled conditions, what is not applicable to dynamic simulation where dynamic stall behavior is dominant. Reference [4] studies the histeretic behavior resultant from the use of different stall models. The main contribution to hysteretic behavior of the lift coefficient is not only the separeted flow effect. Theodorsen's potential flow model [18] for a two dimensional oscillating thin plate indicated that the histeretic lift coefficient behavior is related to unsteady wake vorticity potential interference on bound vorticity.

The present work follows traditional UVLM formulation, but including concepts of multi-body dynamics for the definition of position and velocities of points in the wing. Those concepts were already used in the corotational formulation [5, 7] that couples to the present code and are important for the definition of large displacements and rotations. An extension to the above works is the inclusion of a stall model. It is an engineering approach based on observation of post stall behavior of thin wing profiles.

The complete framework is constructed in a way that different aerodynamic and structural solver can be coupled together, even as an internal code or as external libraries. It is intended to be used as a reaserch tool, where new methodologies can be easily added and results compared within a same code structure. With the prescribed rigid body dynamics, the aeroelastic framework is prepared for a future application in flight dynamics aeroelasticity, similar to what is done by [12], for example. An object-oriented programming is used, in similar way as in [8]. With this sort of programming techinique the implementation of aerodynamic vortex-ring element is facilitated by the use of classes that can save and use the element properties efficiently.

The goals of the present work are:

I. Implement an efficient unsteady vortex-lattice code using an object oriented formu-

lation.

II. Investigate the use of a stall model.

III. Present underway development of presented formulation, to extend the applicability to rotary wing models.

In the next sections, the aerodynamic formulation is described. Considerations about the numerical implementation are made, before showing numerical studies.

2. REFERENCE FRAMES FOR LARGE DISPLACEMENTS AND ROTATIONS

As a preparation for the UVLM formulation, the definition of reference frames and associated tranformation are given beforehand. Multi-body dynamics concepts are essential when dealing with large rotational and translational displacements in a moving frame. Some basic transformations involving large-rotations are presented here, following [6] and [14]. The different reference frames and coordinate systems are defined in Fig. 1: (1) an inertial fixed frame of reference IF, defined by vectors $[\mathbf{e}_1, \mathbf{e}_2, \mathbf{e}_3]$; (2) a coordinate system fixed to the body at its initial position, BF_0, defined by vectors $[\mathbf{e}_1^{B0}, \mathbf{e}_2^{B0}, \mathbf{e}_3^{B0}]$; (3) a coordinate system fixed to the body, BF, that rotates and translates in relation to the inertial system $[\mathbf{e}_1^{B}, \mathbf{e}_2^{B}, \mathbf{e}_3^{B}]$; and (4) various local point frames PF, $[\mathbf{e}_1^{P}, \mathbf{e}_2^{P}, \mathbf{e}_3^{P}]$, that can be defined at the 3/4 chord point on an aerodynamic panel, for example.

For the sake of clarity, in the remaining of the text superscripts are used to identify the reference frame in which the vectors are expressed, except when in the IF. For example, $\mathbf{u}^B$ means that the displacement is written in the BF, and only $\mathbf{u}$ means that it is written in the IF. The same applies to the time derivatives.

The moving reference frames are updated at each time and sub-iterations steps, based on prescribed body motions defined instantaneously for each independent degree-of-freedom. The position and orientation of the BF are defined by vectors $\mathbf{X} = \{X_1, X_2, X_3\}^T$ and $\Psi = \{\psi_1, \psi_2, \psi_3\}^T$, both given in relation to the inertial frame. The vector normal to the deformed surface at an arbitrary point on the wing, expressed in the BF, is given by $\mathbf{n}_P^B = n_{Pi}\mathbf{e}_{Bi}$. To represent the same vector in the IF, the following transformation is used:

$$\mathbf{n}_P^I = \mathbf{T}_{BI}\mathbf{n}_P^B, \tag{1}$$

where $\mathbf{T}_{BI}$ is the matrix that transforms the coordinates from the BF to the IF. This transformation matrix can be expressed using the Rodriguez formula [14]:

$$\mathbf{T}_{BI} = \mathbf{I} + \tilde{\mathbf{S}}(\Psi)\sin|\Psi| + 2\,\tilde{\mathbf{S}}(\Psi)^2\sin^2\frac{|\Psi|}{2}. \tag{2}$$

where $\mathbf{I}$ is the 3 x 3 identity matrix, $\tilde{\mathbf{S}}(\Psi)$ is the skew-symmetric (or antisymmetric) matrix of the rotation vector that expresses the BF orientation with respect to the IF, and can be defined by the magnitude of rotation φ and the rotation direction vector $\overline{\Psi}$, resulting in $\Psi = |\Psi|\overline{\Psi}$ [2]. The skew-symmetric matrix of Ψ is given by:

$$\tilde{\mathbf{S}}(\Psi) = \begin{bmatrix} 0 & -\psi_3 & \psi_2 \\ \psi_3 & 0 & -\psi_1 \\ -\psi_2 & \psi_1 & 0 \end{bmatrix}. \tag{3}$$

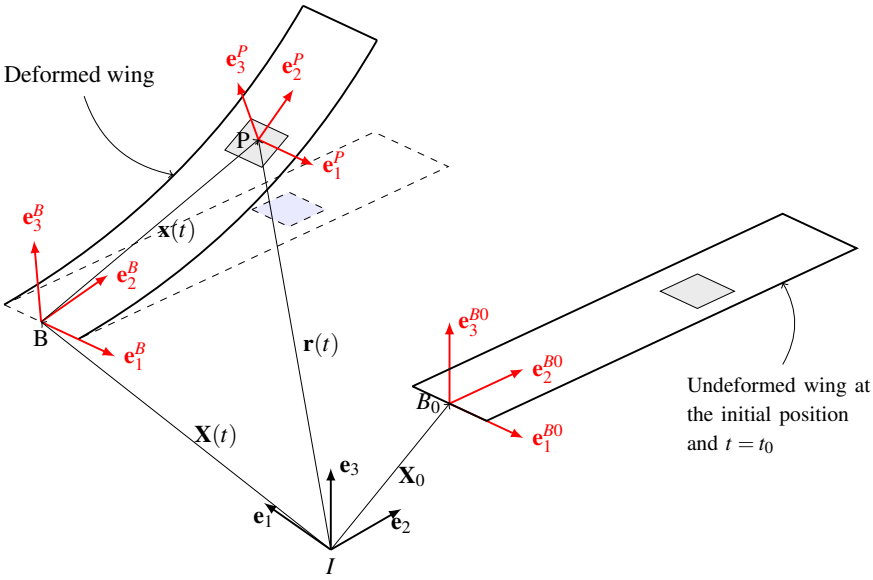

Figure 1. Coordinate systems used in the present work.

The velocity of the BF origin is given by the sum of the linear body velocity and the tangential velocity obtained from the rotational angular velocity:

$$\mathbf{v}_{0BF} = \dot{\mathbf{X}} + \omega \times \mathbf{X} \tag{4}$$

where ω is the BF angular velocity vector of the body frame. It is composed by the time derivatives of the rotation vector components:

$$\omega = \dot{\Psi} = \{\dot{\psi}_1, \dot{\psi}_2, \dot{\psi}_3\}^T. \tag{5}$$

Differentiating Eq. (6), the body frame acceleration is

$$\mathbf{a}_{oBF} = \ddot{\mathbf{X}} + \dot{\omega} \times \mathbf{X} + \omega \times \dot{\mathbf{X}} \tag{6}$$

When deformable bodies are considered, the distance between two arbitrary points on the body does not, in general, remain constant. The expression for the displacement of a point in the wing, thus, need to consider relative displacements in the BF. The displacement in the inertial frame is defined as the difference between the current point position $\mathbf{r}$ and $\mathbf{r}_0$, the initial point position in the IF:

$$\mathbf{u} = \mathbf{r} - \mathbf{r}_0, \tag{7}$$

The current point position itself depends on the position of the BF origin, $\mathbf{X}$, and the present point position in the body frame $\mathbf{x}^B$, what yields to

$$\mathbf{r} = \mathbf{X} + \mathbf{T}_{BI}\mathbf{x}^B, \tag{8}$$

This position is the result of a combination of the initial point position plus the displacement calculated in the BF, what expands Eq. (9) to the form

$$\mathbf{r} = \mathbf{X} + \mathbf{T}_{BI}\left(\mathbf{x}_0^B + \mathbf{u}^B\right), \tag{9}$$

Differentiating the above equation with respect to time, the velocity of a point in the wing is

$$\dot{\mathbf{r}} = \mathbf{v}_{0BF} + \dot{\mathbf{T}}_{BI}\left(\mathbf{x}_0^B + \mathbf{u}^B\right) + \mathbf{T}_{BI}\frac{d}{dt}\left(\mathbf{x}_0^B + \mathbf{u}^B\right). \tag{10}$$

It is demonstrated by [14] that the time derivative of a transformation matrix $\mathbf{T}_{BI}$ is given by

$$\dot{\mathbf{T}}_{BI} = \tilde{\mathbf{S}}(\omega)\mathbf{T}_{BI},, \tag{11}$$

where $\tilde{\mathbf{S}}(\omega)$ is the skew-matrix defined in Eq. (3). Since the position $\mathbf{x}_0^B$ is constant with time, then $d(\mathbf{x}_0^B)/dt = 0$. Using Eqs. (6) and (11), Eq. (10) yields to

$$\dot{\mathbf{r}} = \dot{\mathbf{X}} + \omega \times \mathbf{X} + \tilde{\mathbf{S}}(\omega)\mathbf{T}_{BI}\mathbf{x}_0^B + \tilde{\mathbf{S}}(\omega)\mathbf{T}_{BI}\mathbf{u}^B + \mathbf{T}_{BI}\dot{\mathbf{u}}^B. \tag{12}$$

3. UNSTEADY VORTEX-LATTICE METHOD

The vortex lattice methods is based on the assumption of incompressible irrotational flow allowing the existence of a potential function that is a single scalar variable, namely the velocity potential, being the gradient of such a quantity $\mathbf{V} = \nabla\Phi$. Assuming incompressible flow and the velocity potential, velocities components and a time and space invariante density function, continuity equation is reduced to Laplace equation as,

$$\nabla^2\Phi = 0 \tag{13}$$

The solution of this linear partial differential equation request the knowledge of boundary conditions. Her it is assumed zero normal flow across the wing surface, represented by:

$$\nabla(\Phi + \mathbf{v}) \cdot \mathbf{n} = 0 \tag{14}$$

where $-\mathbf{v}$ is the surface's kinematic velocity and $\mathbf{n}$ is the vector normal to the lifting surface. The Laplace equation is a full potential operator, not being obtained by any linearization hypothesis based on small disturbances. For this reason the non-linear kinematic boundary condition relation presented before shall be considered, and it can be applied to the representation of lifting surfaces under large displacements. Since the Laplace equation is a linear operator, solution of this equation can be linearly combined in a superposition sense. Aerodynamic singularity functions (vortex, source, dipoles) are solution of Laplace equation. The UVLM assumes the lifting surface can be represented by a vortex singularity distribution. The are two types of vortex singularity to be used in the UVLM, horseshoe vortex and vortex ring.

The vortex ring approach has an important characteristic that allows its use in unsteady formulations, that is, both the lifting surface and the wake are divided into vortex elements. Bound vortex elements are placed over the lifting surface while shed vortex elements are convected from the trailing edge forming the wake. Induced velocity flow field might convect the shed vortex elements allowing its roll up. Time marching solution for solving Laplace equation assumed the lifting surface displacements as a function of time, in other word unsteady kinematic boundary conditions updating the position of all elements at each time step.

The lifting surface is divided into elements containing vortex ring singularities, as seen in Fig. 2. Vortex lines are superposed to a panel element forming the vortex ring. The forward line is placed at 25% element chord position, and the rearward line is placed at 25% chord of the next element. The lateral lines run on top of the element edges. This way, the collocation point is equally distant to both sides, but remains in the center of the vortex ring element.

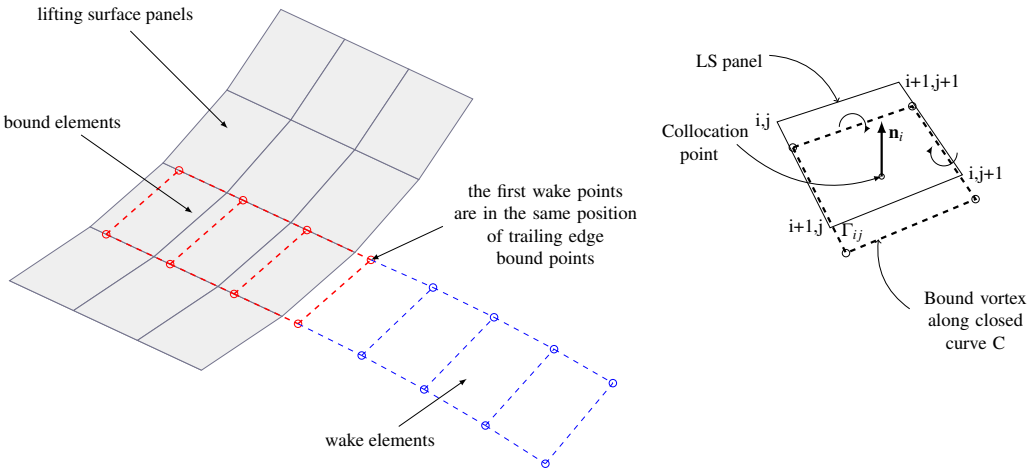

Figure 2. A vortex ring element imposed on a rectangular wing panel.

The velocity induced by the closed curve C is expressed as an integral along the curve:

$$\mathbf{w}_c = \frac{\Gamma}{4\pi}\int_C \frac{d\mathbf{l}\times\mathbf{r}}{r^3}dC \tag{15}$$

The induced velocity $\mathbf{w}_{ij}$ is the influence on a element i by an element j, and is expressed as

$$\mathbf{w}_{ij} = \left(\frac{1}{4\pi}\int_{Cj}\frac{d\mathbf{l}\times\mathbf{r}_i}{r_i^3}\right)\Gamma_j = \overline{\mathbf{w}}_{ij}\Gamma_j. \tag{16}$$

This integration can be substituted by a summation of the velocity induced by the four sides of the vortex ring by assuming an unit induced velocity due to the vortex ring element by means of Biot-Savart law, defined as,

$$\overline{\mathbf{w}}_{ij} = \sum_{k=1}^{4}\left\{\frac{1}{4\pi}\frac{\mathbf{r}_{pi}\times\mathbf{r}_{qi}}{\left|\mathbf{r}_{pi}\times\mathbf{r}_{qi}\right|^2}\left[\mathbf{r}_{0i}\left(\frac{\mathbf{r}_{pi}}{r_{pi}}-\frac{\mathbf{r}_{qi}}{r_{qi}}\right)\right]\right\}_k \tag{17}$$

where $p = 2,3,4,1$ and $q = 1,2,3,4$ in this order, representing the order of vortex ring corner nodes. If the lifting surface is divided into m vortex ring elements, the potential at a given control point placed at an element i will the result of a linear sum of all the influences from other elements in the domain: bound and shed, the latter hereafter named as wake elements. Once the gradient in Eq. (14) is a linear operator, and can be split into two separate terms:

$$\nabla\Phi = \nabla\Phi_B + \nabla\Phi_w, \tag{18}$$

where Φ_B is the potential of bound elements and Φ_w is the potential of the shed wake.

Defining the velocity induced by the wake as $\nabla\Phi_w = \mathbf{w}_w$, and $\mathbf{v}$ as an external flow velocity $-\mathbf{v}_{ext}$, Eq. (14) can now be rewritten as:

$$(\nabla\Phi_B + \nabla\Phi_w + \mathbf{v})\cdot\mathbf{n} = (\nabla\Phi_B + \mathbf{w}_w - \mathbf{v}_{ext})\cdot\mathbf{n} = 0 \tag{19}$$

The total local velocity is defined to include explicitly all velocities contribution at a given control point. The resulting velocity is composed by the wake induced velocity and the total induced velocity as

$$\mathbf{v}_{res} = \mathbf{w}_w - \mathbf{v}_{tind}. \tag{20}$$

Taking into consideration that a panel is moving in an inertial system and that the lifting surface is also moving in relation to the body frame, the total induced velocity is actually computed as:

$$\mathbf{v}_{tind} = \mathbf{v}^P_{kin} - \mathbf{v}^P_{wind} = \mathbf{v}^P_{panel} + \mathbf{v}^P_{body} - \mathbf{v}^P_{wind}, \tag{21}$$

where $\mathbf{v}_{wind}$ is the velocity of a local wind (atmospheric) and $\mathbf{v}_{kin}$ is the kinematic velocity. The kinematic velocity is composed by the local velocity of the lifting surface due to deformation or imposed rotations, $\mathbf{v}_{panel}$, and body velocity due to an imposed movement $\mathbf{v}_{body}$. Linear and angular body velocities are included in the above expression, as per the definition of $\mathbf{v}_{body}$ in Eq. (6). The superscript P means that the above resulting velocity components have to be established in the panel reference frame. The calculation of the kinematic velocities depend on the moving frames formulation, explained in section 2.

Finally, the expression for the resulting velocity is given by:

$$\mathbf{v}_{res} = \mathbf{w}_w - (\mathbf{v}^P_{panel} + \mathbf{v}^P_{body}) + \mathbf{v}^P_{wind}, \tag{22}$$

where the negative sign at the kinematic velocity terms means that the equivalent flow velocity is in opposite direction of the panel movement, in the panel coordinate system.

With this resulting velocity defined, a linear equation system is assembled, where the bound element vorticity strength Γ_j is the unknown:

$$(\overline{\mathbf{w}}_{ij} \cdot \mathbf{n}_j)\, \Gamma_j = -\mathbf{v}_{resj} \cdot \mathbf{n}_j. \tag{23}$$

In matrix notation, the above system is given by:

$$\overline{\mathbf{A}}\, \mathbf{g} = \mathbf{f}_v. \tag{24}$$

The matrix $\overline{\mathbf{A}}$ is the aerodynamic influence coefficients matrix, $\mathbf{g}$ is the vector of circulation strength at the control points of bound vortex elements, and $\mathbf{f}_v$ is the right-hand side vector. The time dependency is included in the boundary conditions by means of panel normal vector and wake position history, and relates to a geometry update at each time step.

3.1. Free wake approach

With the bound elements vorticity computed from the solution of eq. (23), the next step is the computation of free wake shed vorticity and vortex ring elements spatial position. The physical explanation for the existence of a shed wake is explained by Kelvin's Theorem, where it is stated that the total circulation in the flow field need to be zero. In other words, once a bound vorticity exists, a shed vorticity need also to exists in opposite direction such that thee total vorticity present in the flow field tends to vanish.

The free wake solution also implies on a term known as "wake rollup" [10], what defines the procedure in which the wake is set free to move according to the local induced velocity, resulting in a rolling condition at the wake free edges. The induced velocity at a point "i" due to the vorticity of a vortex-ring element j can be defined using the element definition in eq. (17). The induced velocity $\mathbf{w}$ at a wake point i is calculated after defining the vorticity strength on all lifting surfaces and wake elements. It is a summation of velocities $\mathbf{w}_{Bij}$- induced velocity on point i by an bound element j - and velocities $\mathbf{w}_{wik}$ - induced velocity on point i by a free element k:

$$\mathbf{w}_i = \sum_j \mathbf{w}_{Bij} + \sum_k \mathbf{w}_{wik} \tag{25}$$

In the present implementation, where the body movements are expressed in an inertial frame, the induced displacement is added to the inertial parcel: $\mathbf{u} = \mathbf{u}_I + \mathbf{u}_{ind}$. The updated position of each wake point is then given by:

$$\mathbf{x}_w = \mathbf{x}_0 + \mathbf{u}_I + \mathbf{u}_{ind}$$

where $\mathbf{x}_0$ is the initial point position, $\mathbf{u}_I$ is the inertial displacement, passed from the last bound element grid points, and $\mathbf{u}_{ind} = \mathbf{w}\,\Delta t$. This procedure, however, is time consuming, and the computational cost increases with longer wake sheets.

3.2. Pressure and forces

The pressure distribution is found using the unsteady Bernoulli equation. Following the notation of [10], it is expressed as

$$\frac{p_{ref} - p}{\rho} = \frac{Q^2}{2} - \frac{v_{ref}^2}{2} + \frac{\partial \Phi}{\partial t}_{body} \tag{26}$$

where p is the local fluid pressure, Q is the magnitude of the local fluid velocity, and the subscript ref indicates a reference field condition. This equation is based on the resulting velocity at each panel that depends on the lifting surface displacement history and on the solution of the potential equation, obtained from Eq. (24). The pressure difference between the upper and lower surfaces is then

$$p_{ref} - p = \rho \left[\left(\frac{v_t^2}{2} \right)_u - \left(\frac{v_t^2}{2} \right)_l + \left(\frac{\partial \Phi}{\partial t} \right)_u - \left(\frac{\partial \Phi}{\partial t} \right)_l \right] \tag{27}$$

The terms of this equation are calculated as presented in [10]. Considering the tangential derivative of thin airfoil potential, the tangential velocities v_t in the $\mathbf{e}_1$ and $\mathbf{e}_2$ directions are defined from

$$\begin{aligned} v_{t_1} &= \mathbf{v}_{res} \cdot \tau_1 \left(\pm \frac{\partial \Phi}{\partial \tau_1} \right) = \mathbf{v}_{res} \cdot \tau_1 \left(\pm \frac{\Gamma_{ij} - \Gamma_{i-1,j}}{2\Delta c} \right), \\ v_{t_2} &= \mathbf{v}_{res} \cdot \tau_2 \left(\pm \frac{\partial \Phi}{\partial \tau_2} \right) = \mathbf{v}_{res} \cdot \tau_2 \left(\pm \frac{\Gamma_{ij} - \Gamma_{i,j-1}}{2\Delta b} \right), \end{aligned} \tag{28}$$

where the $\pm$ sign stands for upper and lower surfaces, respectively, Δc is the panel chord and Δb is the panel span. From the relation between the potential jump and vorticity across the lifting surface and wake [10], the velocity-potential time derivative is obtained as

$$\pm \frac{\partial \Phi}{\partial t} = \pm \frac{\partial}{\partial t} \sum_{k=1}^{j} \frac{\Gamma_k}{2}. \tag{29}$$

A manipulation using definitions in Eqs. (28) and (29), yields a discretization of Eq. (27) as:3

$$\Delta p_k = \rho \left\{ \mathbf{v}_{res}(t) \cdot (\tau_i \Delta \Gamma_i) + \mathbf{v}_{res}(t) \cdot (\tau_j \Delta \Gamma_j) + \frac{\partial}{\partial t} \Gamma i, j \right\}, \tag{30}$$

where $\Delta\Gamma_i = (\Gamma_{ij} - \Gamma_{i-1,j})/\Delta c_{ij}$ and $\Delta\Gamma_j = (\Gamma_{ij} - \Gamma_{i,j-1})/\Delta b_{ij}$, and the Δp_k is the pressure applied to the k^{th} panel considering both tangential velocities potential derivatives. The resulting force vector at a panel is obtained simply by multiplying the pressure by the area and the panel normal vector:

$$\mathbf{f}_k = \Delta p_k \, S_k \, \mathbf{n}_k \qquad . \tag{31}$$

The total force is obtained from a summation on all elements, and the force coefficients c_F obtained by dividing this force by the total lifting surface are multiplyed by an equivalent dynamic pressure:

$$\mathbf{c}_F = \frac{2}{\rho v_{ref}^2 S_T} \mathbf{f}_T, \tag{32}$$

where S_T is the total area and $\mathbf{f}_T$ is the total force vector. This force coefficient vector is given in the same coordinate system used to define $\mathbf{n}_k$ in Eq. (31).

3.3. Effective angle of attack

The definition of an effective angle of attack is necessary for the later implementation of a stall model, since it relies on this information. Here, the local angle of attack is defined as the angle between the local resultant velocity and the panel orientation. This velocity vector is the same used at the core of the UVLM, defined in Eq. (20) and used in the RHS of the linear system of equations used to solve for the vorticity strength distribution.

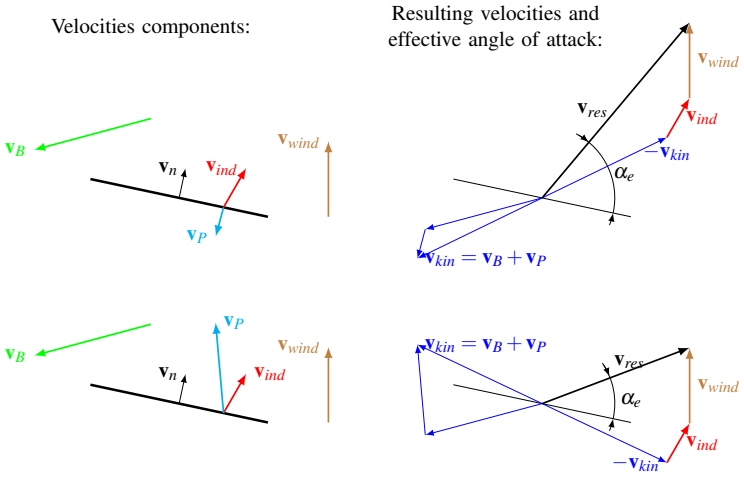

Figure 3. Definition of element resulting velocity and local effective angle of attack.

The effective angle of attack is then obtained from an internal product between the resulting velocity $\mathbf{v}_{res}$ and the panel chordwise direction:

$$\alpha_e = \cos^{-1}\left(\frac{\mathbf{v}_{res} \cdot \mathbf{e}_1}{|\mathbf{v}_{res}|\,|\mathbf{e}_1|}\right) \tag{33}$$

3.4. Stall model

Stall models have been developed for taking into account the associated separated flow contributions to a given unsteady aerodynamic loading. Many stall models have been developed for compressible flow devoted to rotary wing aerodynamic loading calculations. However, for low speed aerodynamic applications, due to the semi-empirical nature of such models, they are inappropriate for the present application.

Figure 4 shows the static $C_L \times \alpha$ curves for a flat plate wing with increasing aspect ratios compared to the 2π reference line and a reference curve for a flat plate section. The results shown for the vortex lattice solution do not contain stall corrections. For higher aspect ratios and small angles of attack, the curves are very close to the 2π line, what is not verified

for AR=4. Increasing the angles, there is an increasing distance to the reference line, what is expected due to tip vortex effects. Comparing to the reference curve for thin plates, what is noticed is exactly that some stall effects are necessary to adjust the results.

For the sake of expediency regarding the implemented numerical aerodynamic model, the method of choice to overcome this limitation is based on an engineering approach. This approach consists in applying a relaxation factor to the C_P obtained on a bound vortex-ring element after the VLM time-step solution. A proportional penalty factor p_s is applied to the C_P of an element k:

$$C_{P,stall} = p_s C_P, \qquad \text{where} \quad p_s = \begin{cases} 1 & , \text{if } \alpha_e \leq \alpha_{cut} \\ \varepsilon_\alpha \dfrac{\alpha_{cut}}{\alpha_e} & , \text{if } \alpha_e > \alpha_{cut} \end{cases} \tag{34}$$

and α_e is the bound element effective angle of attack defined in the previous section and α_{cut} is an arbitrary stall angle that has to be defined based on experiments or higher-order numerical methods. To complement the formula, a factor ε_α, defined as the post-stall penalty factor, is used to adjust the response for larger angles. A schematic description of this process is shown in Fig. 5.

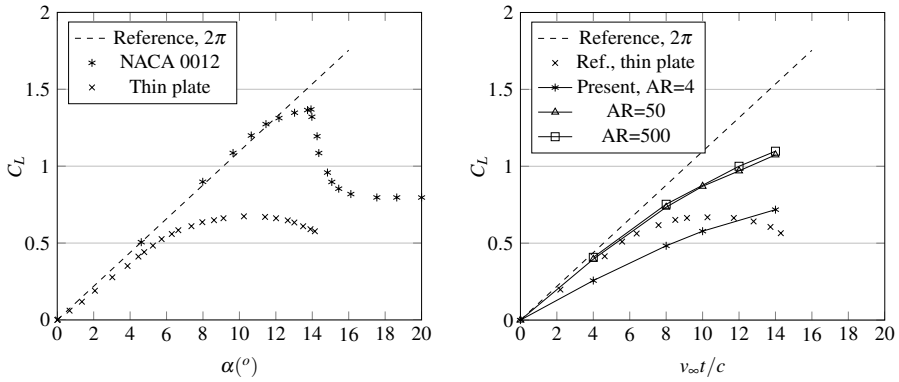

(a) (b)

Figure 4. (a) Quasy-static $C_L \times \alpha$ curves. (b) Results obtained with present approach, without stall limitations.

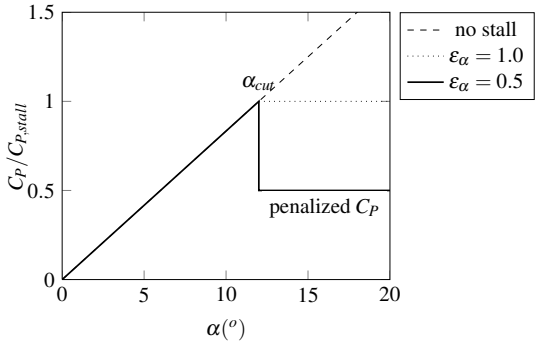

Figure 5. Schematic of penalized C_P as function of panel effective angle-of-attack.

In summary, the presented strategy considers mainly the hysteretic behavior associated to potential flow effects. The separation effects is included as quasi-steady stall behavior based

on the principle of the instantaneous lift efficiency loss, as far as the panel effective angle of attack α_e reaches α_{cut}, i.e., the airfoil static stall angle of attack.

4. NUMERICAL FRAMEWORK

The code is implemented in c++, what allow to take the advantage of object orientated programming technique. Also, it created in order to facilitate the management of information throughout the code, but still be a light and fast code. Classes and data structures are used though the code to handle input and output data, and, more important, simulation objects.

The information handling is important for an efficient code, and in the present case special attention has been given to that. The model is constructed using a single text input file, with command fields that ocuppy one or more lines with 80 characters. Inside the code, an generic input class is used to read the input file and save inside special command data structures. Another dedicated function translates the command structures to the dedicated internal variables. The LAPACK software package [11], linked to the code as a library, brings efficiency to the solution of linear systems.

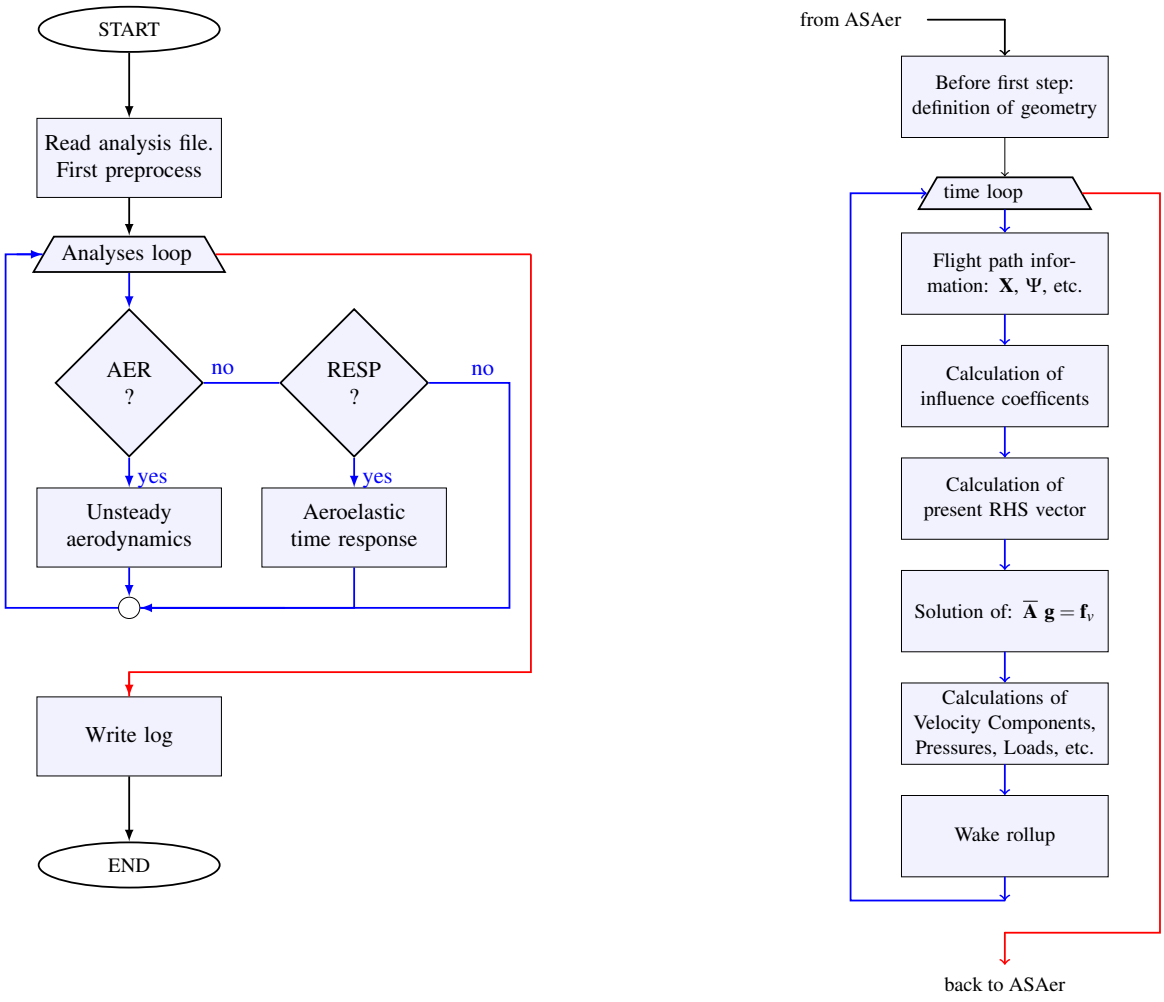

Figure 6. Numerical framework: on the left, the ASAero main flowchart; on the right, the UVLM flowchart, placed inside the Unsteady aerodynamics block in ASAero.

4.1. Aerodynamic model discretization

The aerodynamic model is defined using the concept of aerodynamic macro-elements (AME), which are continuous surfaces that are divided into a finite number of aerodynamic panels, according to parameters defined by the user. These macro-elements are associated with a set of structural FE, and an internal routine identifies which are the nodes contained in both sides. The interpolations are then applied separately to each set AME/FE.

A c++ class is created for the vortex-ring element, and two derived classes are used to deal with bound and wake elements. The bound elements need to handle more information, like the orientation at its center, for example. Also, the effective angle of attack need to be calculated only at a bound element, and not at a wake one. Because of that, the function to update bound elements at each time step are more complex than that of an wake element.

The original undeformed meshes is saved and is used as reference during the simulation. Displacement matrices are created for the complete aerodynamic model: one for the corner points of the wings panels, a second for the bound elements corner points, and a third for the wake elements corner points. These matrices are updated at each time step, following the formulation in section 2. The transformation between inertial and body fixed system is always required for the definitions of RHS vector in the aerodynamic side and for the corotational formulation used in NLAMS.

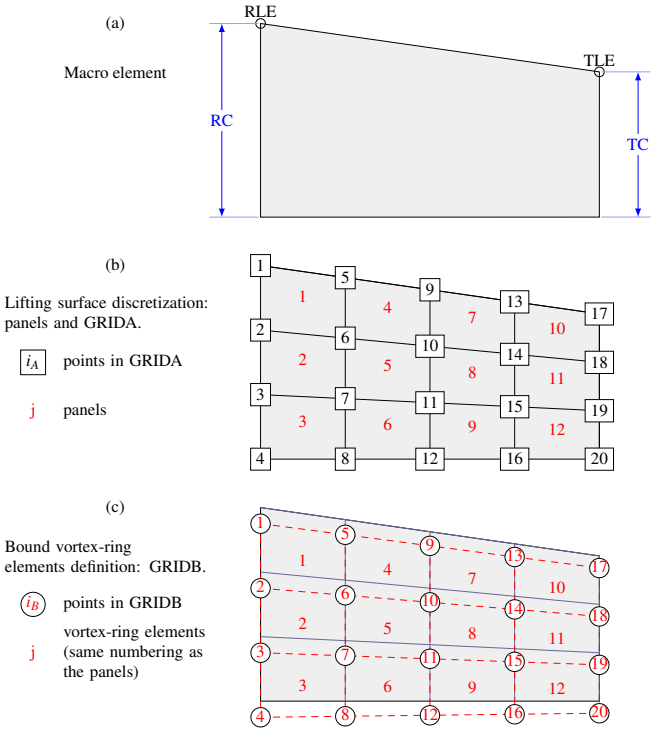

Figure 7. Discretization steps in the Vortex-Ring method, defined by coordinate of root leading egde (RLE), tip leading edge (TLE) points, root (RC) and tip (TC) chords.

4.2. Considerations on the wake

The loading results are dependent on the wake panel chord and in the shedding procedure. It was noticed that the same bound element chord should be used in the wake elements. Taking into consideration a wing that moves in the $\mathbf{e}_{I1}$ direction at a constant velocity $\mathbf{v}$, the wing trailing edge suffer a displacement equal to $x_1 = V_{inf} * \Delta t$ and the the shed wake elements

have a chord value of x_1. To maintain the wake panel chord homogeneous in the complete wake, the time step has to be defined as

$$\Delta t = \frac{1}{V_{inf}} \left(\frac{c}{n_x} \right) \tag{35}$$

where c is the wing chord and n_x is the number o panels in the wing.

The wake shedding follows a modified procedure, compared to the version described in [10]. Here, the wake is created based on a desired number of main chords: $L_w = n_c \; c_l$, where n_c is the number of chords and c_l is the lifting surface chord. The number of panels is then:

$$\begin{aligned} n_{pw} &= n_{wy} \, n_{wx} \\ n_{wy} &= n_{ly}, \text{ the number of spanwise panels in the lifting surface} \\ n_{wx} &= \frac{L_w}{c_{pw}}, \text{ the wake length divided by the wake panel chord} \end{aligned} \tag{36}$$

At $t = 0$, all the wake points are concentrated at the wing trailing edge. As the wing starts moving in the $-\mathbf{x}_1$ direction, the line of wake points attached to wing follows it, and the rest remain in the initial position. At $t = 2dt$ the second line of wake points follows the wing, too, a so forth. After a number of time steps equal to the number of wake points in the chordwise direction ($npwx$), all the wake is already following the wing.

A special procedure was created to evaluate the differences $\Delta\Gamma_i$ and $\Delta\Gamma_j$ in eq. (30), because they depend on the type of discretization used to model the aerodynamic panels: single or multiple surfaces. The differences $\Delta\Gamma_i$ and $\Delta\Gamma_j$ are then established based on the panel position inside this macro-element.

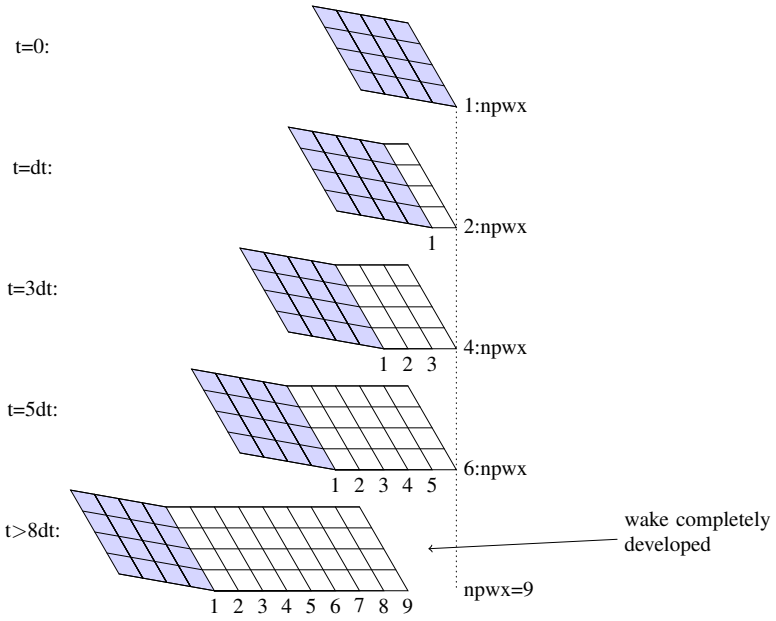

Figure 8. Simplified scheme of the wake shedding procedure as view from a wing under a linear movement in the x_1 direction (no rotations), at the beginnig of simulation for prescribed wake condition.

5. NUMERICAL STUDIES

5.1. UVLM framework verification

For validation purposes, the example 1 of chapter 13 of [10] is used. This is an example of steady-state flight, with a solution for transient lift of a rigid wing. It means that no flight dynamics or aeroelasticity is taken into account, but the wing remains fixed and undeformed. The results are presented for a wing with the following parameters: rigid flat rectangular wing; aspect ratio from 4 to 200 ($= \infty$); angle of attack of 5^o; discretization of 13 panels along the span and 4 along the chord.

In the first time step the gradient $\partial\Phi/\partial t$ is large, and convergence is achieved soon after that. The suggested value for the time step in the reference is $U_\infty \Delta t/c = 1/16$. However, the numerical investigation showed a dependency of the time step with the the size of the wake panel exists. It is necessary to adjust the time step value so that the chord of each wake panel has to be the same of the wing panels, using the formula 35. Results then obtained compare very well with reference values, as seen in Figure 9.

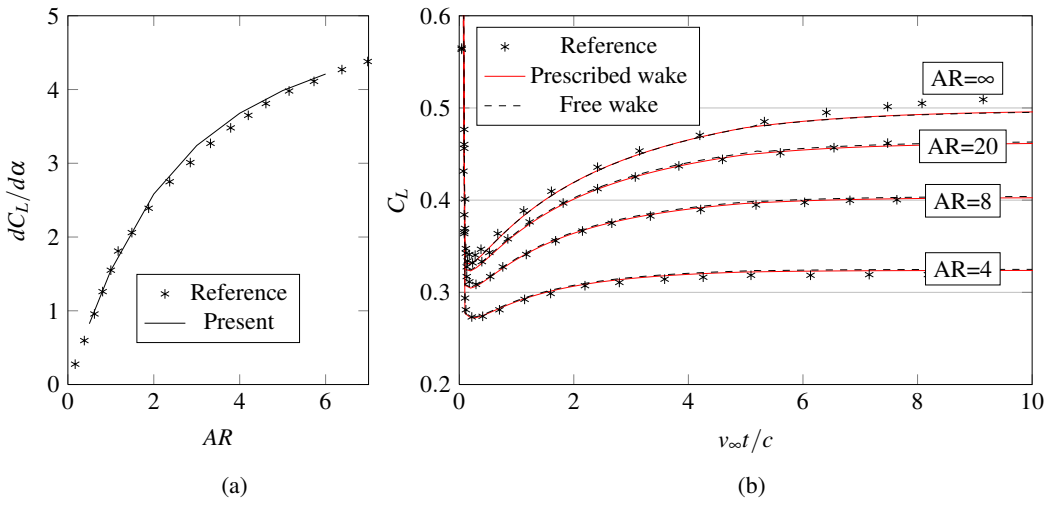

Figure 9. (a) Comparison of $dC_L/d\alpha$ for an increasing value of Aspect ratio. (b) Convergence of C_L with time step. Reference values from [10].

The above model is used for convergence and computational time studies, varying number of panels in the chord and spanwise directions, as well as wake length and, most important, the use of free or prescribed wake conditions. For all the simulations, a time step of 0.01s is used, for $v_{ref} = 10m/s$ and total simulated time of $1s$. Table 1 shows results for simulations with free wake and prescribed wake approaches. The studies show that the dependence of the C_L on the discretization in the spanwise direction is small. On the other hand, there's almost no difference between the use or not of free wake approach. When comparing the simulation time, however, the differences are big. The time is highly influenced by two parameters: the number of wake panels and the use or not of free wake procedures. The simulations ran in an Intel(R) Xeon(R) E5430, at 2.66GHz and 64 bit linux system (2.6.32-33-server).

Table 1. Convergence studies for a flat plate wing under sudden acceleration, free and prescribed wake simulations (AR=4, v_{ref}=10m/s, chord=1m).

n_y	n_x	n_c	C_L	t (s)	wake
8	10	5	0.3270	30.0	
10	10	5	0.3225	55.0	Free
14	10	5	0.3172	89.0	
20	10	5	0.3130	170.0	
8	10	10	0.3293	71.0	
10	10	10	0.3247	110.0	Free
14	10	10	0.3193	237.0	
20	10	10	0.3151	447.0	
8	10	5	0.3271	6.0	
10	10	5	0.3266	10.0	Prescr.
14	10	5	0.3172	17.0	
20	10	5	0.3130	39.0	
8	10	10	0.3294	10.0	
10	10	10	0.3248	12.0	Prescr.
14	10	10	0.3193	25.0	
20	10	10	0.3151	51.0	

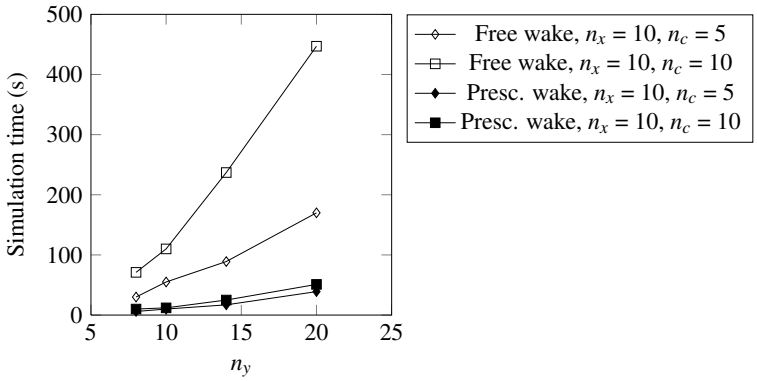

Figure 10. Comparison of simulation time for a the rectangular flat plate.

5.2. Stall model verification

Hysteresis loops are used to verify the applicability of the proposed approach. A response for hysteresis loop of a rigid flat plate is obtained by applying a sinusoidal variation to the nominal angle of attack:

$$\alpha = \alpha_A \sin(\omega_A t) \tag{37}$$

where α_A is the oscillation amplitude, $\omega_A = 2\,\pi\,f_A$, the oscillation frequency in rad/s, with f_A given in Hz. The results shown below were obtained from $\alpha_A = 15^o$ and values of f_A from 0.2 to 1.0 Hz, as an initial investigation. Also, in all simulations, α_{cut} has been simply set to 12^o and ε_α to 0.5.

Fig. 11 shows hysteresis loops of a moderate aspect ratio flat plate, comparing with a quasi-static $C_L \times \alpha$ curve of a thin plate typical section. It is possible to observe that a hysteresis is established around the quasi-static response. The post-stall behavior is very dependent on the chosen value of ε_α, and more investigation is needed on this topic. Adjustments need to be made in order to adjust the curves to experimental values. In a further investigation, the same flat plate with $AR = 10$ is subjected to different f_A = 0.2, 0.5 and 1.0 Hz, with results shown in Fig. 12. It is seem that the hysteresis effects become stronger with higher frequencies, as expected. On the other side, very small f_A approximate the response to a quasi-static behavior. The influence of aspect ratio is related to the C_L magnitude, due to the wing tip vortex shedding. Fig. 13 shows 4 different hysteresis loops for $AR = 4$ and $AR = 10$, and simulation parameters. The maximum C_L is smaller for smaller AR, but the hysteresis loops follow the same general behavior for both AR at the same f_A.

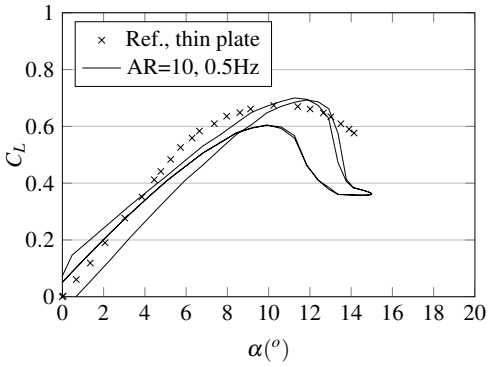

Figure 11. Comparison of a quasi-steady $C_L \times \alpha$ curve for a thin plate and a hysteresis loop for an oscillating flat plate (AR=10, $f_A = 0.5Hz$).

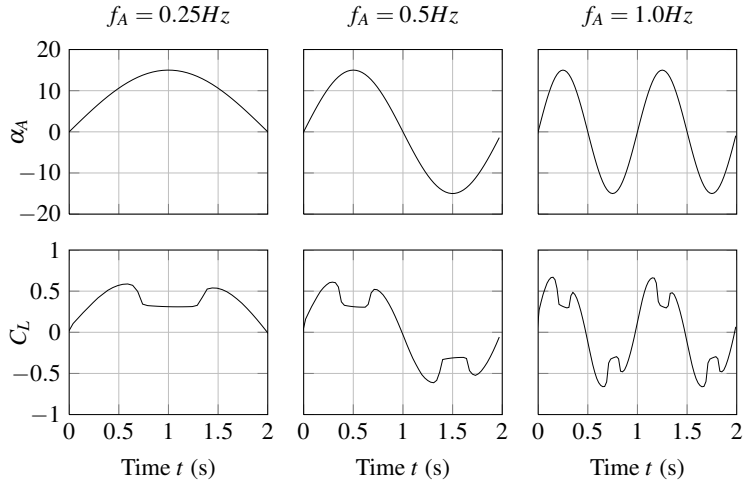

Figure 12. Stall results for a flat plate under a cyclic variation of prescribed angle of attack α.

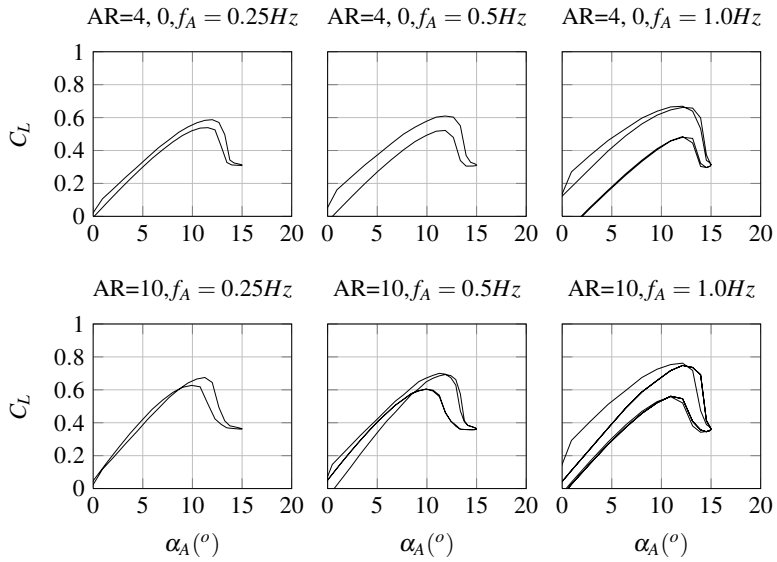

Figure 13. Hysteresis loops for oscillating flat plates under $\alpha = \alpha_r \sin(\omega_r t)$ and different parameters.

To understand C_P distribution on the lifting surface, Fig. 14 has snapshots of four

steps in the ascendant part of the nominal α with values of p_s. In this figures, the brown color means $p_s = 1.0$ and blue grades represent areas where the factor is below 0.5, what means that the local α_e is above α_{cut}. Even for small α, the trailing edge already presents high α_e (Fig 14, what is slowly spreading through the surface as the nominal α increases. For α lower than α_{cut} at least half the surface has a penalization in C_P, because of resulting induced velocities that take æ to a higher value (Fig. 14 (c)).

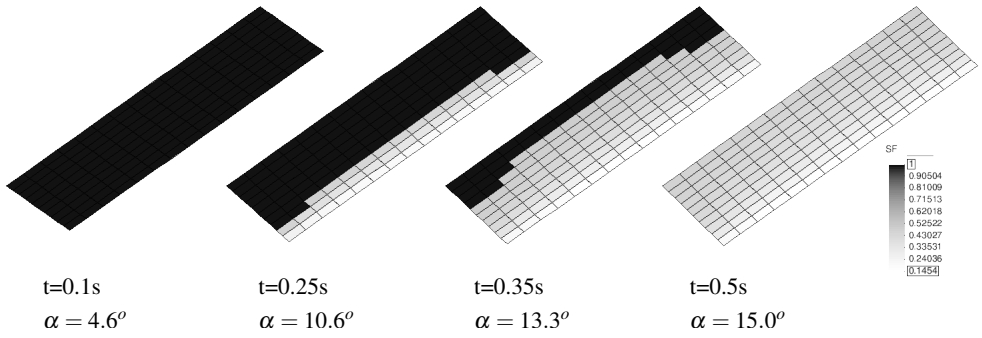

Figure 14. Distribution of penalty factor on the lifting surface at different time steps and different nominal angle of attack.(Model: AR=4)

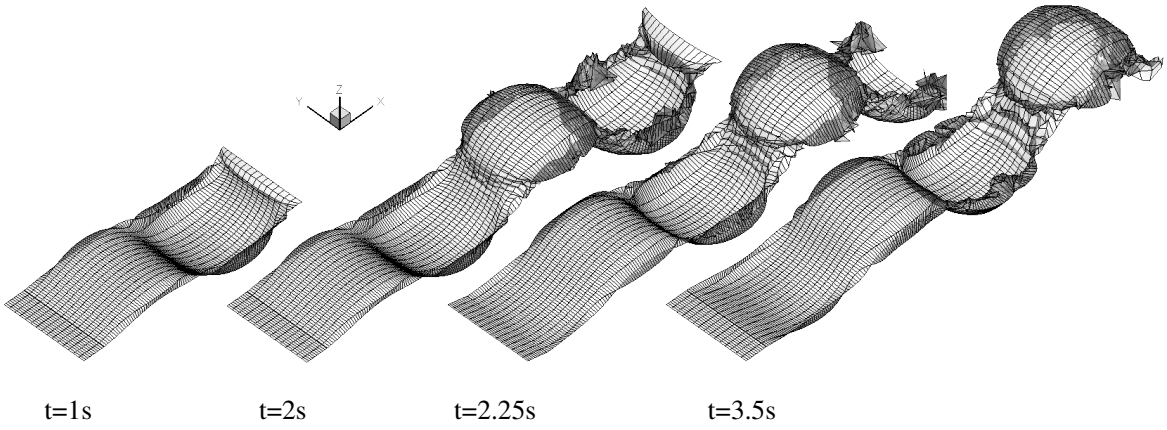

Figure 15. Snapshots for the oscillating flat plate wing (Model: AR=4, L_w=15 chords.)

5.3. Further capabilities under development

Further investigations efforts are underway, besides the aeroelastic results shown in [7]. The idea is to demonstrate the code's ability to deal with multiple lifting surfaces and very large rotations. Here, a rotary model, equivalent to a double blade propeller, is shown. Even if force values are not yet validated, other features can be tested: modeling of two separated aerodynamic macro-elements (AME); application of very large rotations; application of positive and negative incidence angles.

Figure 16(a) shows the dimensions of the rotary wing model. The two surfaces are rigid, what means that no structural model is coupled to the aerodynamics. It is composed by two surfaces, with a gap at the root, and placed symmetrically around the x_1 axis. A torsion is applied to the model, by means of two different incidence angles at the wing root and wing tip. These angles are applied antisymmetrically for each surface. The prescribed motion at

the wing root is

$$\mathbf{u} = \{-v_\infty t \quad 0 \quad 0\}^T \text{(m)} \qquad \Psi = \{\psi \quad 0 \quad 0\}^T (\pi/180^o)(rad/s),$$

what means that the wing is moving in the $-x_1$ direction and rotating around the same axis at a speed of ψ degrees per second. This movement is shown in Fig. 16(b).

Figure 17 shows four snapshots of simulation results for a model discretized into 15 $\times$ 5 bound elements and wake length of 20 chords, $v_\infty = 5m/s$ and $\psi = 18.85(rad/s) = 1080(^o/s)$. It is seen that the wake develops and follows the surfaces, with the free wake condition well captured. However, further investigations are necessary to validate forces and moments results, allowing the simulation of the aerodynamic loading on propellers or wind turbine blades, for example.

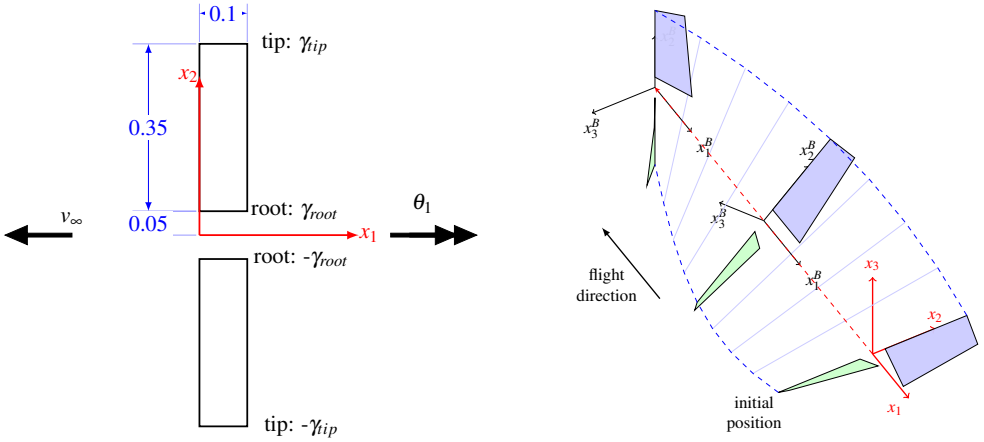

Figure 16. (a)Rotary wing model, defined with different incidence angles at root and tip. (b) Applied body dynamics: translation in the -x_1 direction and rotation around the same axis.

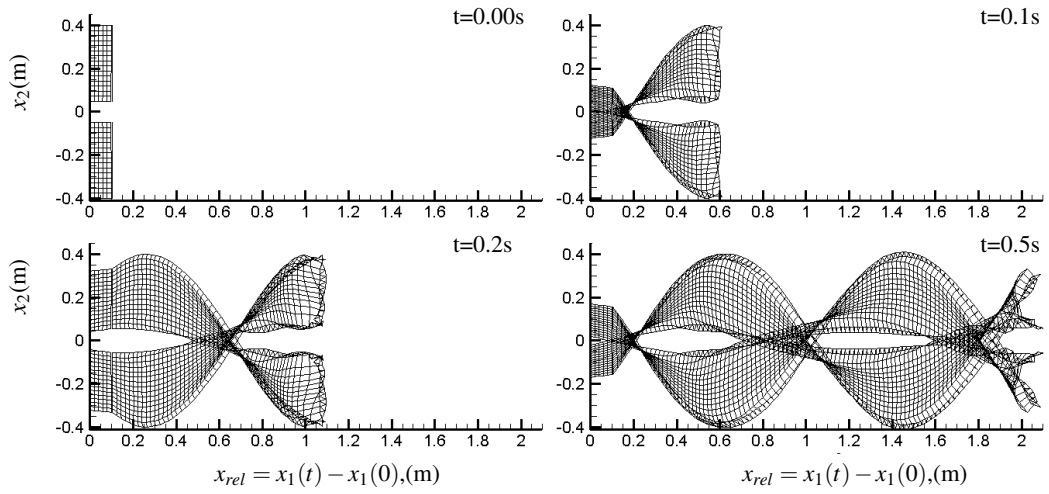

Figure 17. Snapshots of the rotaty model for a free wake simulation.

6. CONCLUSION

An UVLM implementation is presented, with capabilities of large rotations and displacements. This UVLM code is part of larger aeroelastic framework dedicated to the study

of highly flexible plate-like wings subject to large displacements at a low computational cost. In the aerodynamic part of the problem, the addition of a stall model through penalization parameters allowed the identification hysteretic behavior, what is not possible when no stall is considered. Simulations of rigid flat plate showed that the lift coefficient can be well represented even around the stall region. Hysteresis loops simulations showed the ability to capture a lift lag expected for oscillating wings. Comparisons with experimental results are necessary to define the two parameters defined for the separated flow approximated model: the stall angle α_{cut} and the post-stall penalty factor ε_{α}.

The computer code is created using an objected-oriented programming technique, with definition of classes to deal with input files, aerodynamic vortex-ring elements and output data. This technique brings a series of advantages in development time and for future code expansion to add new features, because of the modular architecture. The use of libraries like LAPACK brings efficiency to the solution of linear systems. The code implementation resulted in fast simulations, where a 1 second simulation of surface with 200 panels and wake length of 10 chords can be done in less than 1 minute for a prescribed wake simulation or less than 7.5 minutes when considering free wake.

Future work include experimental tests of rigid plates to adjust the stall parameters, and validation of rotary wings models. Also the coupling between multiple lifting surfaces composed of structural finite element models and the vortex ring elements control points may allow the simulation of more complex models, from complete aircraft to multiple blades rotary wing configurations.

Acknowledgments

The first and second authors acknowledge the partial support from the Instituto Nacional de Ciência e Tecnologia - Estruturas Inteligentes em Engenharia, INCT-EIE, the Conselho Nacional de Desenvolvimento Científico e Tecnológico, CNPq, and also the Fundação de Amparo à Pesquisa do Estado de Minas Gerais, FAPEMIG, from Brazil. The first author was also partially supported by the University of Michigan's Active Aeroelasticity and Structures Research Laboratory.

7. REFERENCES

[1] Aono, H., Chimakurthi, S. K., Wu, P., Sällström, E., Stanford, B. K., Cesnik, C. E. S., Ifju, P., Ukeiley, L., and Shyy, W. (2010). A computational and experimental study of flexible flapping wing aerodynamics. In *48th AIAA Aerospace Sciences Meeting Including the New Horizons Forum and Aerospace Exposition 4 - 7 January 2010, Orlando, Florida*.

[2] Arnold, V. I. (1989). *Mathematical Methods of Classical Mechanics*. Graduate Texts in Mathematics. Springer-Verlag New York Inc.

[3] Banerjee, S. P. (2007). *Aeroelastic Analysis of Membrane Wings*. PhD thesis, Virginia Polythechnic Institute and State University, Blacksburg.

[4] Bierbooms, W. (1992). A comparison between unsteady aerodynamic models. *Journal of Wind Engineering and Industrial Aerodynamics*, 39(1-3):23–33.

[5] Chimakurthi, S. K., Stanford, B. K., Cesnik, C. E. S., and Shyy, W. (2009). Flapping wing cfd/csd aeroelastic formulation based on a co-rotational shell finite element. In *50th AIAA/ASME/ASCE/AHS/ASC Structures, Structural Dynamics, and Materials Conference 17th AIAA/ASME/AHS Adaptive Structures Conference 11th AIAA*.

[6] Crisfield, M. A. (1990). A consistent co-rotational formulation for non-linear, three-dimensional, beam-elements. *Comput. Methods Appl. Mech. Eng.*, 81:131–150.

[7] de Souza, C. E., Silva, R. G. A., and Cesnik, C. E. S. (2012). Nonlinear aeroelastic framework based on vortex-lattice method and corotational shell finite element. In *53rd Structures, Structural Dynamics, and Materials Conference (SDM)*. AIAA.

[8] Fritz, T. E. and Long, L. N. (2004). Object-Oriented Unsteady Vortex Lattice Method for Flapping Flight. 41(6).

[9] Katz, J. (1981). Large-scale vortex-lattice model for the locally separated flow over wings. In *AIAA 14th Fluid and Plasma Dynamics Conference*.

[10] Katz, J. and Plotkin, A. (2001). *Low Speed Aerodynamics*. Cambridge University Press, Cambridge, UK, 2nd. edition.

[11] LAPACK (2012). Lapack linear algebra package - http://www.netlib.org/lapack/.

[12] Palacios, R., Murua, J., and Cook, R. (2010). Structural and aerodynamic models in nonlinear flight dynamics of very felixble aircraft. *AIAA Journal*, 48:2648–2659.

[13] Seber, G. and Bendiksen, O. O. (2008). Nonlinear flutter calculations using finite elements in a direct Eulerian-Lagrangian formulation. *AIAA Journal*, 46(6):1331–1341.

[14] Shabana, A. A. (2005). *Dynamics of Multibody Systems*. Cambridge University Press, third edition edition.

[15] Stanford, B. and Beran, P. (2009). An updated lagrangian shell and vortex lattice aeroelastic framework for flapping wings. In *IFASD 2009*.

[16] Stanford, B. K. and Beran, P. S. (2010). Analytical Sensitivity Analysis of an Unsteady Vortex-Lattice Method for Flapping-Wing Optimization. *Journal of Aircraft*, 47(2):647–662.

[17] Su, W. and Cesnik, C. E. S. (2010). Nonlinear aeroelastic simulations of a flapping wing micro air vehicle using two unsteady aerodynamic formulations. In *51st AIAA/ASME/ASCE/AHS/ASC Structures, Structural Dynamics, and Materials Conference*, number AIAA-2010-2887, pages 1–22.

[18] Theodorsen, T. (1935). General theory of aerodynamic instability and the mechanism of flutter. Technical Report NACA-TR-496, NACA.

[19] Wang, Z. (2004). *Time-Domain Simulations of Aerodynamic Forces on Three-Dimensional Configurations, Unstable Aeroelastic Responses, and Control by Neural Network Systems*. PhD thesis, Virginia Polytechnic Institute and State University.